IEEE Access
Multidisciplinary | Rapid Review | Open Access Journal

Received September 26, 2021, accepted October 9, 2021, date of publication October 13, 2021, date of current version October 25, 2021.

Digital Object Identifier 10.1109/ACCESS.2021.3119668

A Compact Reconfigurable 1-D Periodic Structure in GaAs MMIC With Stopband Switching, Dual-Band Operation and Tuning Capabilities

IRFAN SHAHID[1], (Member, IEEE), DUSHMANTHA N. THALAKOTUNA[2], (Senior Member, IEEE), DEBABRATA K. KARMOKAR[3], (Senior Member, IEEE), SIMON J. MAHON[1], AND MICHAEL HEIMLICH[1], (Senior Member, IEEE)

[1]Faculty of Science and Engineering, School of Engineering, Macquarie University, North Ryde, NSW 2109, Australia
[2]School of Electrical and Data Engineering, University of Technology Sydney, Ultimo, NSW 2007, Australia
[3]UniSA STEM, University of South Australia, Mawson Lakes, SA 5095, Australia

Corresponding author: Irfan Shahid (irfan.shahid@hdr.mq.edu.au)

ABSTRACT This paper presents a systematic study of a compact and reconfigurable periodic structure in GaAs MMIC technology. Compactness is achieved by the introduction of spiral inductors in a conventional unit cell without disturbing the reactive loading mechanism. The proposed architecture exhibits a 28.3% wider stopband with 62.6% smaller footprint compared to a conventional structure. The compactness and bandwidth improvement in the proposed structure is explained with the help of dispersion and circuit analysis. The reconfigurability built into the design using PIN diodes allows stopband switching, dual-band operation and tuning capabilities with the mere use of a single reactive load in its unit cell. To the best of the authors knowledge, it is the first time a reconfigurable MMIC implementation is realized using the proposed structure or even the conventional design. As a guide to design, sensitivity analysis to filter performance is presented for important structure parameters. Switching element parasitics are discussed in two ways: firstly, with the design and measurement of structures with idealized switching conditions and in second, with the circuit and full-wave EM modelling of the finite periodic structure with the actual PIN diodes. The on-chip measurements of the fully reconfigurable filter show excellent agreement with simulations.

INDEX TERMS Periodic structure, electromagnetic bandgap (EBG), GaAs MMIC, reconfigurable circuits, tunable filters, PIN diodes.

I. INTRODUCTION

With the advent of 5G, cognitive radio and ultra-wideband systems, demand for the reconfigurable radio frequency (RF) front ends is on the rise [1]–[4]. Devices that can adapt themselves to a controlled input are getting popular [5]–[8]. This calls for devices that are multifunctional and offer multiband operation. Filters being an integral part of such RF front ends become more beneficial when they support multiple response types, frequency/bandwidth tuning, band switching, etc. [9], [10].

It is, however, challenging to combine all these reconfigurable attributes in one filter structure. Various reconfigurable filters reported in the literature demonstrate excellent performance when designed for one or two adaptive features at a time. Having more bands over which one can tune results in complex filter structures with compromised performance attributes. For example, the bandstop filter in [11] supports single-band operation with centre frequency tuning in a wide range and stopband rejection level up to 30 dB. In contrast, the filters in [12], [13] offer bandwidth tuning along with frequency tuning with lesser stopband rejections up to 20 dB. Similarly, the filters in [6], [14] demonstrate dual bandstop performance with frequency tuning, and the filter in [15] offers a dual-band operation with bandwidth tuning. Few of the common challenges faced by these filter structures include narrow bandwidths with limited tuning ranges and lack of sufficient rejections in the stopbands [11]–[15], which are among the most desired features when realizing reconfigurable RF front ends.

The associate editor coordinating the review of this manuscript and approving it for publication was Yiming Huo.

This work is licensed under a Creative Commons Attribution 4.0 License. For more information, see https://creativecommons.org/licenses/by/4.0/

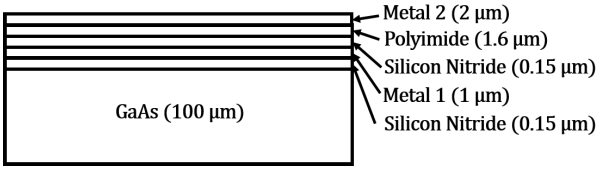

FIGURE 1. The layer definition (with layer thicknesses) of the PIH1-10 MMIC process used for this study.

Electromagnetic bandgap structures (EBG) are popular as they offer deeper stopband rejection with sharper roll-off factors at the bandgap edges [16], [17]. In these structures, bandgap characteristics are achieved by a periodic arrangement of disruptions in the flow of the propagation path [18]. The use of mushroom-like structures under a microstrip line is one way of creating the EBG effect [19]. In a digitally controlled artificial dielectric (DiCAD) structure in CMOS, this effect is created by the cross-coupling offered by several floating metal strips placed under a differential transmission line [41], [42]. One variant of these structures in microstrip arrangement involves using a rectangular patch with a pair of shorting vias in a unit cell to load a microstrip line reactively [20]. Although this structure is used in literature for several circuit and non-circuit applications in microwave frequency bands, it has a large footprint, i.e., bulky circuit design, thereby restricting its use for monolithic millimeter-wave applications. A large footprint can reduce the yield and increase the cost per circuit in MMIC fabrication. To overcome these challenges, it is very important to reduce the overall size of the structure. These circuits offer the possibility of creating the reconfigurable EBGs by changing the state of individual unit cell elements. However, the conventional structure is capable of supporting a single stopband with bandwidth tuning only [21]. Moreover, dual stopband characteristics and additional reconfigurable features are only possible by using multiple reactive loading elements in a unit cell [22]. Furthermore, the reconfigurability of these circuits is only investigated using ideal switching conditions in literature, i.e., without any active components and biasing circuitries [20]–[23].

In this paper, a reactively loaded microstrip line based 1-D periodic structure is proposed and realized in the MMIC environment. The loading to the microstrip line is achieved by means of a capacitively coupled patch and a pair of spiral inductors shorted to the ground. On-chip PIN diodes are used to make the structure reconfigurable. The off-state capacitance of the diodes combined with the leakage capacitance of the reactive load is used to get a second bandgap. Switching between the two bands is achieved by simultaneously switching all the diodes in a finite periodic structure to ON or OFF states. This stopband switching capability of the proposed circuit makes it suitable for the RF front-ends of the half-duplex communications systems. Furthermore, bandgap characteristics of both the stopbands can be discretely tuned by controlling the switching states of individual unit cells. These features make it a suitable candidate for applications requiring suppression of unwanted signals in the adjacent channels.

The rest of the paper is organized as follows. Section II discusses the design of the proposed unit cell. Investigations related to the viability of making the structure reconfigurable, using ideal switching conditions along with detailed parametric study, are discussed in Section III. A detailed account of the on-chip measurements of the proposed reconfigurable EBG filter along with its salient features is presented in Section IV, followed by a concluding discussion in Section V.

II. UNIT CELL DESIGN

In a conventional mushroom type EBG structure, square patches shorted at the center are used to block the propagation of electromagnetic waves [24], [25]. Rectangular patches with vias located at their edges result in a relatively compact EBG structure [26]. However, the realization of these structures is extremely challenging in size constraint MMIC environments, specially for the low frequency applications. To overcome this challenge, a new method to reactively load a microstrip line is proposed that makes use of a relatively smaller patch connected to two spiral inductors. These inductors account for a similar electrical length wound in a tight space resulting in compact periodic structures. Connecting these inductors to the ground plane through vias provide approximately similar path length for the induced EM current to reach the ground, thus resulting in bandgap characteristics in the same frequency band.

To realize this kind of periodic structure and show its efficacy as a reconfigurable filter with multiple adaptive features for millimetre-wave applications, a standard two metal layer MMIC process is selected. The proposed periodic structure is designed using the PIH1-10 GaAs process from WIN Semiconductor Corp., Taiwan which is a standard two metal layer process over a 100 μm thick GaAs substrate. The layer definition for this process is shown in Fig. 1. In this process, metal-1 layer with the thickness, t_1, of 1 μm is laid over a thin layer of (0.15 μm) Silicon Nitride on the GaAs wafer. Metal-2 has a thickness, t_2, of 2 μm and is isolated from metal-1 with the help of a 0.15 μm thick layer of SiN and a 1.6 μm thick layer of polyimide. The thick metal can be realized by combining metal-1 and metal-2, resulting in an approximate thickness of 3.1 μm. This process supports plated back vias with the thick pad dimensions of $P_X \times P_Y$ as 60 μm $\times$ 90 μm and with an elliptical gold-plated hole having dimensions of $V_X \times V_Y$ as 30 μm $\times$ 60 μm.

Conventionally, in a unit cell, a longitudinal microstrip line with width W_m is laid on metal-2. Under this line, a transversal patch with dimensions as $W_P \times L_P$ is made on metal-1, as shown in Fig. 2(a). The distance between the edge of the unit cell and the patch is S, such that total unit cell length $L_{UC} = L_P + 2S$. In the proposed periodic structure unit cell, a relatively shorter patch is used with width W_P' and is connected to two spiral inductors on each side, as shown in Fig. 2(b). These inductors are realized using thick metal

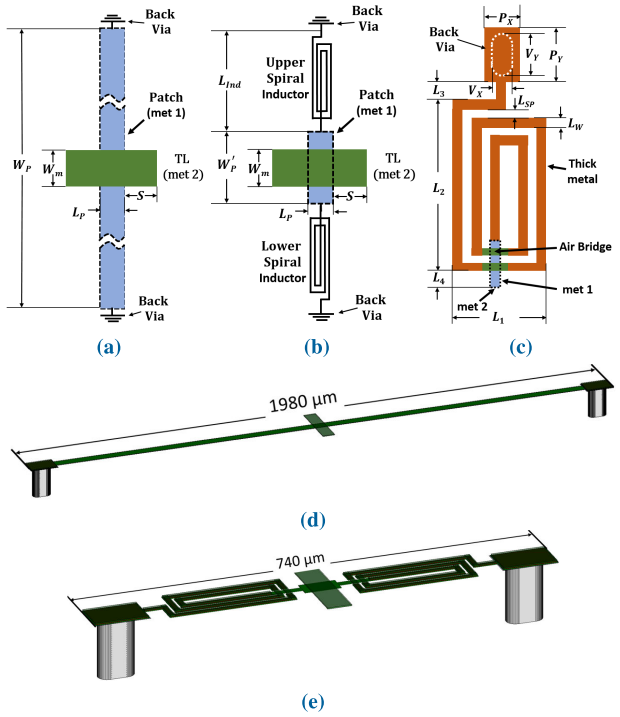

FIGURE 2. Unit cell of the 1-D periodic structure. (a) Schematic of the top view with the conventional shorted patch structure (not to scale). (b) Schematic of the top view with spiral inductors (not to scale). (c) Enlarged view of the spiral inductor and back via on the layout. (d) 3-D view of the conventional unit cell (not to scale) and (e) 3-D view of the proposed unit cell.

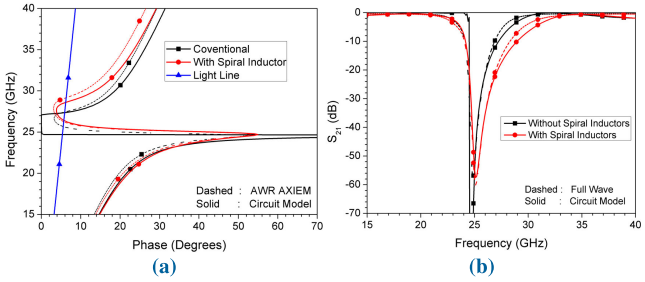

FIGURE 3. (a) Unit cell dispersion diagram. (b) Full-wave simulation results showing the bandgap behaviour exhibited by conventional structure and the proposed structure. The circuit component values for the spiral inductor are $L_S = 1.18$ nH, $C_3 = 0.00448$ pF, $C_S = 0.0112$ pF, $C_{sub1} = 0.01$ pF, $C_{sub2} = 0.01$ pF, $R_S = 2.53\ \Omega$, $R_{sub1} = 50037\ \Omega$ and $R_{sub2} = 22289\ \Omega$. For conventional loading element as $L_{patch} = 1.18$ nH and $C_3 = 0.00448$ pF. Other common circuit values are $C_1 = 0.00371$ pF, $C_2 = 0.0216$ pF, $L_1 = 0.057$ nH and $L_{via} = 0.012$ nH.

with line width as L_W, spacing between spiral segments as L_{SP} and other important parameters marked as L_1 to L_4, as shown in Fig. 2(c). The total via to via distance in the proposed unit cell is $W'_P + 2L_{Ind}$, where, $L_{Ind} = L_2 + L_3 + L_4$. The number of spiral segments shown in Fig. 2(c) are 10 and are referred to as L_N. 3-D views of the conventional and the proposed unit cell are shown in Fig. 2(d) and (e), respectively. This shows that the proposed unit cell significantly reduces the unit cell dimensions in the lateral direction, making it suitable for MMIC implementation.

A. DISPERSION ANALYSIS

The propagation mechanism of the unit cells in Fig. 2(a) and (b) are studied with the help of the dispersion diagram, which is derived using AWR EM simulated data. For dispersion analyses, the unit cell is simulated as a two-port network in the AWR AXIEM simulator. The resulting S-parameters are used to calculate the propagation constant, γ, with the help of ABCD (transmission) matrix coefficients [27], as given below:

$$\gamma L_{UC} = (\alpha + j\beta)L_{UC} = cosh^{-1}\left(\frac{A+D}{2}\right) \quad (1)$$

where, α is the attenuation constant and β is the phase constant. For the dispersion diagram, we are interested in the imaginary part of γL_{UC}, which is expressed in degrees.

The unit cell parameters for the conventional patch structures used for this study are $W_m = 40\ \mu$m, $L_P = 30\ \mu$m, $W_P = 1800\ \mu$m, $S = 75\ \mu$m, $L_{UC} = 180\ \mu$m and via dimensions as mentioned before. The dispersion diagram shows the presence of bandgap between the first two propagating modes, i.e., 24.55 GHz and 27.3 GHz (10.6% fractional bandwidth centred at 25.9 GHz), as shown in Fig. 3(a). To obtain comparable performance using the proposed unit cell, a small patch width, $W'_P = 60\ \mu$m, is used with inductor dimensions as $L_1 = 80\ \mu$m, $L_2 = 210\ \mu$m, $L_3 = L_4 = 20\ \mu$m, $L_N = 10$, $L_W = 10\ \mu$m and $L_{SP} = 10\ \mu$m. The proposed unit cell shows a bandgap between 24.73 GHz and 28.68 GHz (14.8% fractional bandwidth centred at 26.7 GHz) with relatively compact unit cell width, i.e., 740 μm as compared to 1980 μm (including two back vias), as shown in Fig. 2(d) and (e). It is worth mentioning that the proposed unit cell not only offers a 62.6% size reduction of the structure but also offers 28.3% improvement in gap bandwidth.

B. CIRCUIT ANALYSIS

The equivalent circuit model of a conventional structure having a rectangular patch with two shorts is reported in [26] and is further investigated to have more insight into the circuit in a monolithic environment. The proposed equivalent circuit is developed by incorporating the effect of reactive loading on the microstrip line due to spiral inductors. Fig. 4 shows the circuit model for the proposed unit cell in Fig. 2(b). Since the centre of transversal patch and longitudinal microstrip line are aligned and are symmetric about the center of the structure, therefore, the equivalent circuit model of the structure is also symmetric. The microstrip line on each side of the loading patch is approximated with the help of inductance L_1 and a parallel plate capacitance C_1. The inductance L_1 can be approximated using the formula for the self-inductance of a straight rectangular bar [28] and is given as Eq. (2)

$$L_1(nH) = L_{UC}\left\{ln\left(\frac{L_{UC}}{R_1}\right) - 1 + \frac{2R_1}{L_{UC}}\right\} \times 10^{-4} \quad (2)$$

$$R_1 = 0.2235(W_m + t_2) \quad (3)$$

where, all the dimensions are in μm.

The interaction between the microstrip line and the patch is represented by parallel plate capacitance C_2. Furthermore,

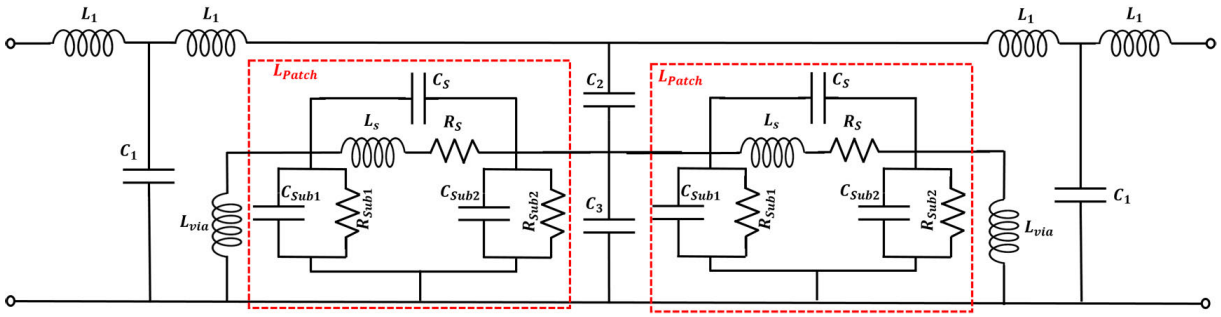

FIGURE 4. Equivalent circuit model approximation for the unit cell in Fig. 2(b).

the parallel plate capacitance between the patch and the ground plane is represented by C_3. The initial values for capacitances C_1, C_2 and C_3 can be approximated by using parallel plate capacitance formulas. The shorting via on each side is represented by an inductance L_{via}. For this analysis, foundry supplied values of L_{via} are used. The effect of the spiral inductor on the structure performance is approximated with the help of a relatively simpler 1-π model [29], [30]. This model gives reasonable accuracy up to the self-resonant frequency (SRF) of the spiral inductor. In this model, L_s and R_s represent the equivalent series inductance and resistance values, respectively. C_s caters for the through capacitance between the neighbouring metal segments of the inductor. Furthermore, R_{sub1} and R_{sub2} are the substrate leakage resistances, and C_{sub1} and C_{sub2} are the substrate leakage capacitances. Values for these lumped components are extracted using the full-wave simulation of the inductor in AWR AXIEM simulator as a two-port network. Then, Y-parameters are used to calculate the circuit values [29], [30] using Eq. (4)

$$\left.\begin{aligned} L_s &= \frac{1}{\omega} imag(-1/\overline{Y}) \quad C_s = \frac{1}{\omega} imag(-\overline{Y}) \\ C_{sub1} &= \frac{1}{\omega} imag(y_{11} + \overline{Y}) \quad C_{sub2} = \frac{1}{\omega} imag(y_{22} + \overline{Y}) \\ R_{sub1} &= 1/real(y_{11} + \overline{Y}) \quad R_{sub2} = 1/real(y_{22} + \overline{Y}) \\ R_s &= real(-1/\overline{Y}) \quad \overline{Y} = (y_{12} + y_{21})/2 \end{aligned}\right\} \quad (4)$$

where, y is the Y-parameter matrix. These values are extracted for frequency corresponding to $jX = 0$, i.e., self resonance frequency of the inductor. For comparison with the conventional shorted patch structure, the 1-π model of the spiral inductor, in Fig. 4, is replaced by a series inductor L_{patch}, which can be calculated with the help of Eq. (2) using patch dimensions.

An initial estimate of the circuit component values for the two unit cells in Fig. 2(a) and (b) is made using Eq. (2) to (4), and phase constant calculations are done using Eq. (1). A few of the circuit parameter values are slightly tuned, and resulting dispersion diagrams for the proposed and the conventional unit cells are shown in Fig. 3(a). For verification, full-wave simulations of the finite periodic structure consisting of eight unit cells are carried out using the AWR AXIEM simulator. The simulation results are presented in Fig. 3(b), which shows that full-wave simulation results are consistent with dispersion analysis as well as the circuit simulations for both structures.

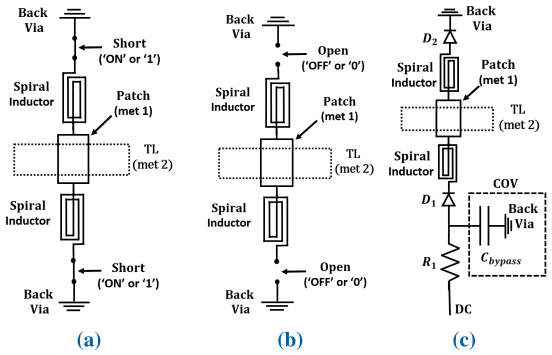

FIGURE 5. Ideal switching conditions used for modelling (a) ON and (b) OFF states in a unit cell. (c) Unit cell schematics of the proposed periodic structure with on-chip PIN diodes and bias circuitry.

III. RECONFIGURABILITY WITH IDEAL SWITCHING CONDITIONS

In this section, the suitability of the proposed periodic structure as a reconfigurable filter is investigated using full-wave analysis. The 'ON' and 'OFF' states of the switching devices are initially modelled using ideal conditions, i.e., with the presence and absence of metal connections, as shown in Fig. 5(a) and (b), respectively. It helps in understanding the performance of a reconfigurable structure and is a widely used technique by researchers for initial design [31], [32]. For simplicity, the ON and OFF states are represented by '1' and '0' states, respectively.

In order to investigate the effect of ON and OFF states on the bandgap performance, two extreme cases were simulated, i.e., first with all unit cells in '1' state and second with all unit cells in '0' state. The schematic diagram of two finite periodic structures, with eight unit cells each, having all the cells in '1' and '0' states are shown in Fig. 6(a) and 6(b), respectively. Full-wave simulation results of the two structures are presented in Fig. 7. Simulation results show that the structure in Fig. 6(a) (with all unit cells in '1' state) offer a bandgap between 24.22 GHz and 28.76 GHz. This stopband is approximately the same as predicted using

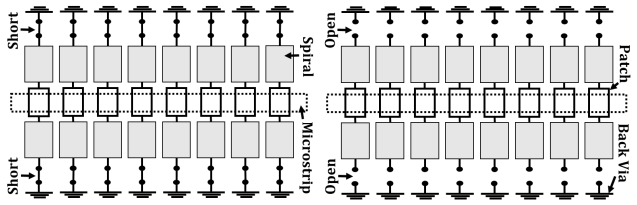

FIGURE 6. Top view of the finite periodic structures with all unit cells (a) connected to ground (short or '1' state) and (b) disconnected from ground (open or '0' state) to simulate ideal switching conditions.

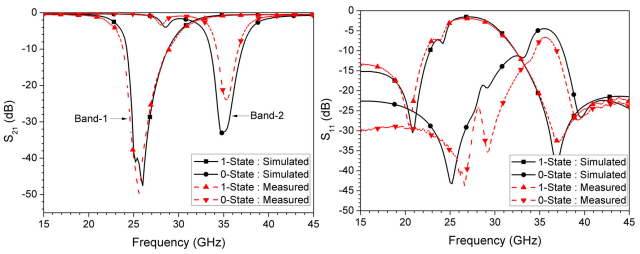

FIGURE 7. Simulated vs measured results for two switching states. (a) Insertion loss. (b) Return loss.

dispersion analysis and is referred to as band-1 with center at f_{c1}. With 8 unit cells, the rejection levels up to 40 dB are achieved in the stopband with better than 15 dB return loss in the passbands. In '0' state, both the spiral inductors in a unit cell are disconnected from the back via leaving the patch and the spiral inductors electronically floating under the microstrip line. This results in reduced reactive loading being offered to the microstrip line which gives rise to bandgap characteristics at slightly higher frequencies. With all unit cells in the '0' state, a bandgap appears between 33.5 GHz and 37.1 GHz, referred to as band-2 with center at f_{c2}. This second bandgap has a band rejection of 30 dB in the stopband. The return loss in this state is better than 12 dB in the upper and lower passbands.

A. PARAMETRIC STUDY ON SPIRAL INDUCTOR PARAMETERS

The effect of important structure parameters on its performance and detailed synthesis scheme to design a filter circuit using this kind of periodic structure on PCB can be found in [33], which takes the system specifications as input and yields 1-D periodic structure geometrical dimensions as output. Detailed discussions on the effect of each structure parameter on its performance can be found in [20], [33]. However, the effect of spiral inductor parameters on the circuit performance is discussed here. Important structure parameters, such as L_N, L_{SP}, L_W, L_2 and unequal inductor length, are individually varied by keeping all other parameters fixed and its effect is simultaneously studied in '1' and '0' states. This study also identifies critical structure parameters for the placement of non-overlapping bandgaps i.e., with higher f_{c2} to f_{c1} ratios. Simulation results obtained from AWR AXIEM simulator are shown in Fig. 8, and a summary of important bandgap characteristics are given in Table 1.

TABLE 1. Summary of bandgap performances resulting from parametric study of important spiral inductor parameters.

Parameter	Value	Band-1		Band-2		f_{c2}/f_{c1}
		f_{c1} (GHz)	FBW %	f_{c2} (GHz)	FBW %	
L_N	6	33.9	20.5	48.5	7.5	1.43
	10	26.6	16.8	35.3	5.8	1.32
	14	19.6	13.0	25.4	3.9	1.29
L_{SP}	5 μm	26.6	16.8	35.3	5.9	1.32
	10 μm	26.9	18.1	37.0	6.8	1.37
	15 μm	27.0	19.3	38.0	6.8	1.41
	20 μm	27.2	20.7	38.9	7.9	1.43
L_W	7 μm	24.5	18.6	34.2	7.6	1.39
	8 μm	25.2	17.6	34.8	6.4	1.38
	9 μm	26.0	17.9	35.9	6.6	1.37
	10 μm	26.8	18.0	37.0	6.8	1.37
L_2	150 μm	33.47	21.5	45.1	7.6	1.34
	200 μm	26.6	17.0	35.3	5.9	1.32
	250 μm	22.2	13.5	29.1	4.3	1.31
L_{2U} (L_{2L}=200)	150 μm	29.8	19.4	41.5	5.7	1.39
	200 μm	26.6	16.8	35.3	6.0	1.32
	250 μm	24.2	14.8	32.9	4.6	1.35

1) NUMBER OF SPIRAL SEGMENTS, L_N

Parametric study on different values of L_N suggests that with an increased number of segments, the spiral inductor presents larger values of inductances. This results in reduced bandgap resonances in both states, as shown in Fig. 8(a). It also presents an increase in the series resistance R_S in each inductor, which increases resistive losses, thus resulting in decreased bandstop rejections.

2) SPACING BETWEEN SPIRAL SEGMENTS, L_{SP}

Changing spacing between spiral segments affects the series capacitance C_S. An increase in L_{SP} results in an increased upper cutoff frequency of band-1, thus increasing the fractional bandwidth, as shown in Fig. 8(b). However, it causes bandgap resonance of band-2 to move up in frequency scale, thus, increasing the second to first bandgap ratio, f_{c2}/f_{c1}, as shown in Table 1. The value of L_{SP} can be carefully chosen to place the second stopband in the band of interest without affecting the resonance of band-1.

3) WIDTH OF SPIRAL SEGMENTS, L_W

Changing the width of spiral segments have a direct effect on the effective inductance offered by the spiral inductor, which results in changed bandgap resonances. Increasing segment width would mean lower inductances, thus bandgap centre frequencies to move up in the frequency scale, as shown in Fig. 8(c).

4) LENGTH OF INDUCTOR, L_2

Increasing L_2 not only increase the total spiral length, which results in increased inductances, but also moves the two vias away from the microstrip line, thus resulting in increased effective path length to the ground as well. The overall effect

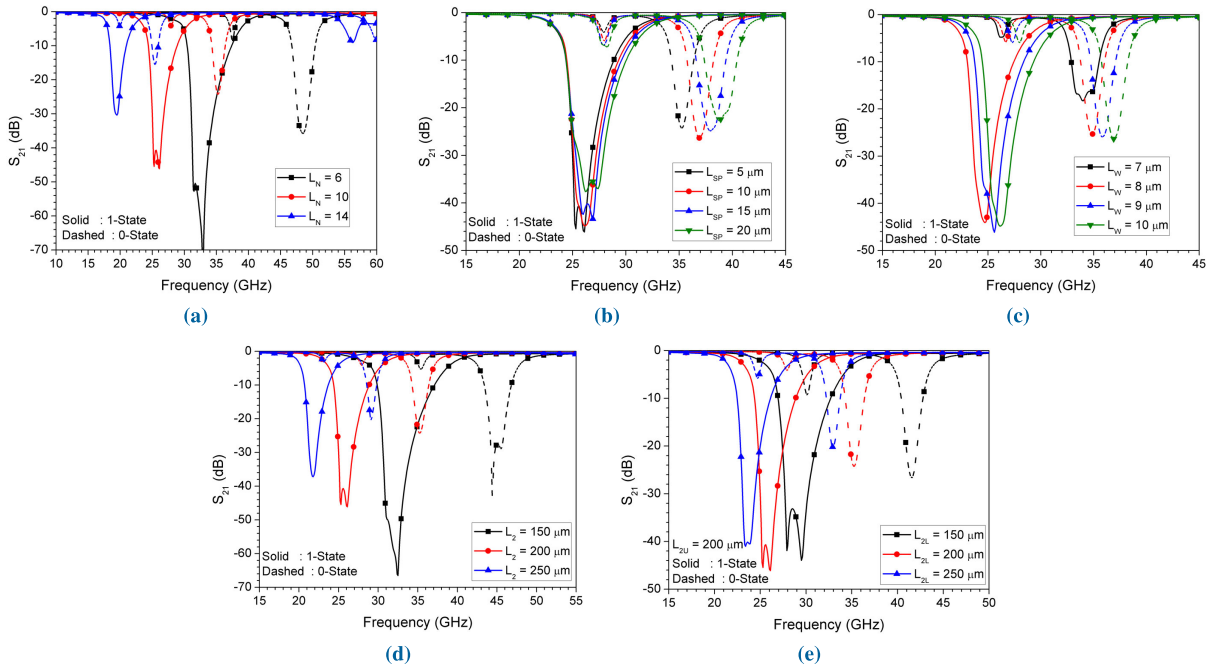

FIGURE 8. S_{21} curves showing the effect on bandgap properties of the structure in '1' and '0' states when (a) L_N, (b) L_{SP}, (c) L_W, (d) L_2 and (e) L_{2L} are individually varied. Baseline parameters used for this study are $W_m = 40$ μm, $L_P = 30$ μm, $W_P = 60$ μm, $s = 75$ μm, $N = 8$, $L_{UC} = 180$ μm, $L_W = 10$ μm, $L_S = 5$ μm, $L_N = 3$, $L_w = 10$ μm, $L_1 = 80$ μm and $L_2 = 210$ μm.

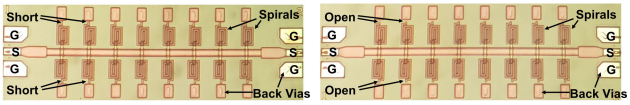

FIGURE 9. Snapshot of the fabricated EBG structures with hard-wired ideal switching conditions for (a) all unit cells shorted to ground, i.e., '1' state and (b) all unit cells floating, i.e., '0' state.

of this is reduced bandgap resonances, as shown in Fig. 8(d). Increased L_2 also results in increased series resistance R_S making the inductive path lossier, which results in reduced bandwidths and lower values of rejections.

5) UNEQUAL INDUCTOR LENGTH

As mentioned earlier, increasing L_2 results in increased path length to ground, thus causing bandgap resonances to shift down in frequency. However, using unequal inductor length, L_2, in two spiral inductors of a unit cell has more effect on band-2 resonance. Its effect is investigated by varying L_{2L} (length of the lower inductor) and keeping L_{2U} (length of the upper inductor) fixed. By doing this, the ratio of second to first bandgap center frequencies, i.e., f_{c2}/f_{c1} can be greatly changed when compared with an equal inductor length case, as shown in Fig. 8(e). As a result, unequal inductor lengths can be used to avoid overlapping of the two bandgaps produced by the proposed periodic structure.

B. EXPERIMENTAL VERIFICATION

In order to ascertain the validity of simulated results, fabrication and measurement of hard wired states of the finite periodic structures are carried out as a proof of concept. Two models with the pre-defined '1' and '0' states of the proposed finite periodic structure were fabricated using WIN Semiconductor's PIH1-10 GaAs process, as shown in Fig. 9. On-chip measurements were carried out using Cascade Microtech's summit 9000 analytical probe station using M/s Infinity's RF probes with ground-signal-ground (GSG) pads having a pitch of 100 μm. The measured results present two distinct bandgaps, which are non-overlapping, as shown in Fig. 7. The simulation and measured results are in good agreement with each other. The proposed structure shows its suitability as a potential candidate for a reconfigurable filter, which can give rise to two distinct bandgaps with a single reactive loading arrangement in a unit cell. The parasitic effects of active devices on the bandgap performance of the structure are discussed in the next section.

IV. PROPOSED RECONFIGURABLE EBG FILTER

This section presents a study on the parasitic effects introduced by the active devices followed by the discussion on proposed reconfigurable EBG filter. On-chip PIN diodes are used as active switching devices which have the ability to switch states in nanoseconds and thus have the potential to make these devices suitable for many cognitive radio and 5G applications. However, these active devices also have adverse effects on the structure performance, which needs to be addressed during design.

A. PARASITIC EFFECTS OF ON-CHIP DEVICES

The effect of active switching devices on structure performance is investigated using industry provided model in the APLAC simulator of AWR Microwave Office. Since both sides of the reactive load in a unit cell are required to be

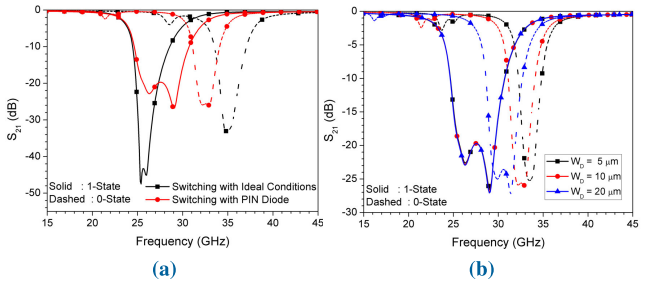

FIGURE 10. (a) S_{21} curves showing the comparison of '1' and '0' states of the proposed periodic structure using PIN diode and ideal conditions. (b) S_{21} curves showing the effect of PIN diode channel width on the structure states.

simultaneously switched ON or OFF. Therefore, the series arrangement of two diodes (D_1 and D_2) is used, as shown in Fig. 5(c). This ensures that both the diodes are in the forward bias mode when the bias is applied, thus, connecting the two spiral inductors to the ground through vias representing '1' state. Similarly, the absence of bias voltage will disconnect the loading elements from the ground, i.e., '0' state. Furthermore, to ensure an RF short in this state and to isolate the reactive load from the effects of the DC supply, a bypass capacitor is used on the DC side of the unit cell. The bypass capacitor is implemented using capacitor-on-via (CoV) with $C_{bypass} = 3.35$ pF and capacitor dimensions of 125 μm $\times$ 65 μm. In this process, a current-limiting thin film resistor (TFR) with a value of 20 Ω and dimensions of 50 μm $\times$ 20 μm is realized to restrict the bias current to 20 mA. For comparison, the diode equivalent area (30 μm $\times$ 40 μm with the channel width $W_D = 10$ μm) is replaced with a metal connection to simulate ideal '1' and '0' states.

The simulation results for the two configurations are shown in Fig. 10(a). In the '1' state, PIN diodes absorb some part of the induced EM energy consumed by the reactive load, thus, resulting in lesser rejections in the stopband. This is evident from 20 dB lesser rejections offered by the actual model when compared to the ideal conditions. Similarly, in '0' state, the off-state capacitance of the PIN diode adds up with the shunt leakage capacitance of the reactive load resulting in decreased bandgap resonances. For example, the actual diode model shifts the center frequency of band-2 to 32.5 GHz from 35.5 GHz (for ideal '0' state), as shown in Fig. 10(a). This off-state capacitance is a function of PIN diode channel width, W_D, and have a direct impact on the center frequency of band-2. Larger channel width of the diode causes band-2 to resonate at lower frequencies with negligible effect on band-1, as shown in Fig. 10(b). Therefore, in order to get non-overlapping bandgaps from the proposed periodic structure, smaller footprint of PIN diodes is required. Since these diodes are not directly connected in the main transmission path, they are capacitively coupled, which only offer an induced EM effect, hence having a minimal effect on the power handling capability of the proposed structure.

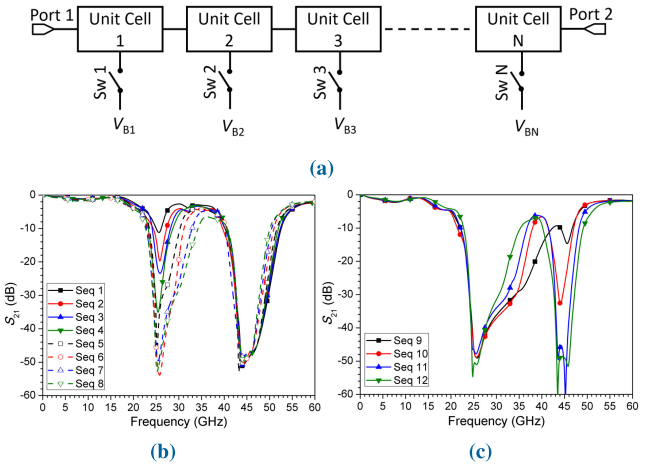

FIGURE 11. (a) Block diagram of the proposed reconfigurable EBG structure. S-parameter curves showing the bandwidth tuning of (b) band-1 and (c) band-2 by presenting different reactive loading profiles to the microstrip line.

TABLE 2. Switching patterns for bandwidth tuning in both bands.

Seq No.	Switching seq	Band-1 (% BW)	Band-2 (% BW)
1	0000000000000100	5	26.5
2	0000000000001100	11.3	27
3	0000000000010010	15	25
4	0010000000100010	20.5	24.6
5	0000010001001010	25	23.7
6	1001001001001001	30	22.4
7	1100110011000100	36	22.9
8	1100110110100010	40	20.6
9	1011111111111111	65	5
10	1111011111011111	55	12.5
11	1110111011101111	50	15
12	1001110110111001	43	20

To further limit these effects, the two PIN diodes in the proposed unit cell are recommended to be placed at the farthest possible distance from the microstrip line.

B. INDEPENDENT SWITCHING OF UNIT CELLS

Independent switching of each unit cell in a finite periodic structure configuration, as shown in Fig. 11(a), offers means of presenting different reactive loading profiles to the microstrip line. The number of unit cells, N, in a periodic arrangement shall give rise to 2^N switching patterns where each sequence has the potential to exhibit an EBG. This arrangement results in bandwidth tuning of both the stopbands in discrete steps each time a unique switching sequence is applied. Selectively switching of unit cells to '1' and '0' states results in bandwidth tuning of band-1 and band-2, respectively. This is demonstrated by simulating a finite circuit having $N = 16$ unit cells using the on-chip PIN diode model data. It can be seen in Fig. 11(b) and (c) that the stop bandwidths of band-1 and band-2 can be tuned in nearly continuous/discrete steps. Here, an approximate step size of 5% is shown for tuning the stop bandwidths of both bands. Salient characteristics of the resulting bandwidths with corresponding switching sequences are given in Table 2. The

proposed reconfigurable EBG filter configuration is useful for the suppression of narrowband as well as wideband signals in the adjacent channels.

C. FABRICATION AND MEASUREMENTS

For validation, the proposed finite structure is fabricated using WIN's PIH1-10 process. In order to achieve non-overlapping stopbands, unequal inductor lengths are used for the two spiral inductors in a unit cell such that $L_{2U} \neq L_{2L}$. Wider bandgaps are achieved using larger microstrip-patch interaction. A total of 16 unit cells are used in this reconfigurable EBG filter prototype to ensure switching flexibility. Keeping in view the limitations in measurements, such as the in-house availability of a DC-probe with limited fingers, a proof of concept is carried out by arranging unit cells into groups for biasing purposes. As a DC-probe with 12 fingers was available with the option to support bias supplies up to 5 cells, therefore, to apply reactively loading profiles in a periodic manner, an even number of bias lines were considered. All 16 cells are biased with the help of four bias lines named $S_1S_2S_3S_4$, as shown in Fig. 12(a). Furthermore, in order to ensure periodicity, each bias line is connected to four unit cells such that $n + 4$ unit cells share the same bias voltage. For example, bias line 'S_1' is shared by unit cell number 1, 5, 9 and 13. In this arrangement, powering on lines 'S_1' and 'S_2' only, would result in a periodic sequence as '1100110011001100' or '..1100..'. Each finger of the DC-probe offers a bias voltage of 3 V with a total forward current of 80 mA. Fabricated model for the proposed reconfigurable EBG filter is shown in Fig. 12(b). The measurement set-up, as discussed in Section III-B, was used for on-chip measurements. A 12 finger DC probe from GGB Industries (MCW-29-3173-3) was used to provide the bias voltages to the device under test. GSG pads were used at the two RF ports, as shown in Fig. 12(b).

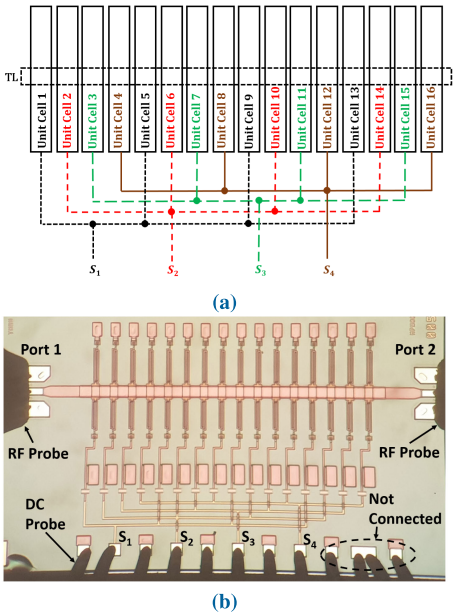

FIGURE 12. (a) Block diagram of finite periodic structure comprising 16 unit cells, where, 4 DC probes are used to fed 4 unit cells in a group. (b) Fabricated reconfigurable EBG structure with probes landed for measurements. Important structure parameters are $W_m = 71$ μm, $L_P = 50$ μm, $W_P = 100$ μm, $S = 35$ μm, $N = 16$, $L_{UC} = 120$ μm, $L_W = 7$ μm, $L_S = 4$ μm, $L_N = 6$, $L_1 = 36$ μm, $L_{2U} = 207$ μm, $L_{2L} = 237$ μm, $L_3 = L_4 = 10$ μm and $W_D = 8$ μm.

1) BAND SWITCHING

When all the PIN diodes are in forward bias mode, i.e., '..1111..' state, the proposed finite periodic structure shows the existence of an EBG with lower and upper 10 dB cutoffs at 19.08 and 38.21 GHz, respectively. The rejections in the stopband are about 55 dB. Moreover, when all the PIN diodes are reverse biased, i.e., '..0000..' state, the reactive loading being offered to microstrip line is changed resulting in bandgap properties at a different frequency band, i.e., from 40.68 GHz to 53.19 GHz with 55 dB rejection in the stopband and better than 1.8 dB insertion loss in the lower passband. Simulated and measured results for '..1111..' and '..0000..' states showing the stopband switching characteristics of the proposed circuits are presented in Fig. 13. As the full-wave simulation of the finite circuit comprising of 32 spiral inductors is computationally very large, the circuit was simulated with a coarse mesh and reduced convergences resulting in a slight deviation between the simulated and measured results. However, the proposed structure exhibits the ability to switch between two stopbands with these two states. The insertion

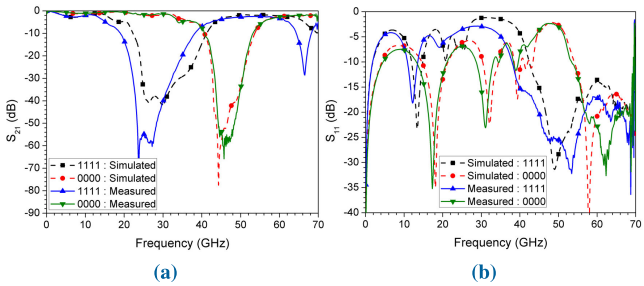

FIGURE 13. Simulated and measured (a) S_{21} and (b) S_{11} curves for '..1111..' and '..0000..' states of the proposed circuit showing its band switching capability.

loss, once these stopbands are switched OFF, is 1.4 dB and 3.1 dB at the bandgap center frequencies of the two bandgaps, i.e., 28.6 GHz and 46.9 GHz, respectively. Using the proposed reconfigurable circuit architecture, this band-switchable stopband filter can be utilized for half-duplex communication system applications.

2) DUAL-BAND OPERATION AND TUNING

The use of four DC lines for switching results in $2^4 = 16$ states which has a total of six unique periodic patterns, i.e., '..1111..', '..0000..', '..1010..', '..1100..', '..1110..', and '..1000..'. The number of unique patterns are limited due to the fact that all the state sequences are not unique. For example, periodic sequence '..1100..' would have similar EBG characteristics as exhibited by sequences '..0011..', '..1001..' or '..0110..', as shown in Fig. 14(a). The measurements

TABLE 3. Measured reconfigurable filter characteristics for different switching patterns.

Switching Patterns	Band-1					Band-2					Remarks
	f_L	f_H	f_{c1}	FBW	SBR†	f_L	f_H	f_{c2}	FBW	SBR†	
$S_1S_2S_3S_4$	(GHz)	(GHz)	(GHz)	(%)	(dB)	(GHz)	(GHz)	(GHz)	(%)	(dB)	
1111	19.08	38.21	28.65	66.78	55	-	-	-	-	-	Single Band
0000	-	-	-	-	-	40.68	53.19	46.93	26.65	55	Single Band
1010, 0101	20.68	33.00	26.84	45.90	45	41.40	50.45	45.92	19.70	60	Dual Band
1110, 1101, 1011, 0111	19.60	35.60	27.60	57.97	50	41.90	48.54	45.22	14.68	40	Dual Band
1100, 0110, 0011, 1001	20.46	32.64	26.55	45.87	40	40.63	50.45	45.54	21.56	55	Dual Band
1000, 0100, 0010, 0001	21.85	29.40	25.62	29.46	25	40.68	51.84	46.26	24.12	55	Dual Band

†: Stopband rejection

TABLE 4. Comparison with the state of the art.

Ref	Response Type	Tuning Mech	Reconfigurable Features		Band-1				Band-2			
			Band-1	Band-2	f_{c1} TR (GHz)	FBW TR MHz / %	SBR (dB)	IL (dB)	f_{c2} TR (GHz)	FBW TR MHz / %	SBR (dB)	IL (dB)
[11]	BSF	Varac	f_c	-	11.3−16.5	-	30	1.5	-	-	-	-
[34]	BPF to BSF	Varac	f_c	-	0.95−1.35	-	15	1	-	-	-	-
[36]	BSF	MEMS	f_c	-	8.5−12.3	-	18	-	-	-	-	-
[37]	BSF	-	-	-	24.5	-	23.1	-	-	-	-	-
[38]	BSF	-	-	-	60	-	33	1	-	-	-	-
[9]	BPF to BSF	Varac	f_c, BW	-	1.9−2.3	2−5.2%$^+$	28	3	-	-	-	-
[12]	BSF	Varac	f_c, BW	-	2.8−3.4	0−3.4%*	20	NG	-	-	-	-
[35]	BSF	PIN	f_c, BW	-	6.87−7.15	8.8−13.4%$^{\&}$	12	1.93	-	-	-	-
[13]	BSF	LC	f_c, BW	-	4.9−5.4	22.2−36.7%*	23	NG	-	-	-	-
[14]	Dual BSF	Varac	f_c	f_c	1.27−1.57	-	13.9	NG	1.98−2.34	-	14.3	0.4
[6]	Dual BSF	Varac	f_c	f_c	0.51−0.85	-	20	NG	0.72−1.17	-	12	NG
[10]	Dual BSF	Varac	f_c	f_c	1.47−1.84	-	33	NG	2.7	-	10	NG
[39]	Dual BSF	-	-	-	30	-	35	2.5	80	-	25	2.5
[3]	Dual BSF	VO_2	Band Switching		28.2	-	15	2	35	-	18	1
[40]	Dual BSF	MEMS	Band Switching		50	-	34	-	60	-	38	-
[15]	BPF to BSF	Varac	BW	BW	-	6.5−13.2%$^{\#}$	15	1	-	1.5−3.6%$^{\#}$	15	1
This Work	Dual BSF	PIN Diodes	f_c, BW Band Switching	f_c, BW	25.6−28.6	0−66.8%$^{\&}$	55	1.8	45.2−46.9	0−26.6%$^{\&}$	55	3.1

BSF = Band Stop Filter, BPF = Band Pass Filter, TR = Tuning Range, FBW = Fractional Bandwidth, SBR = Stopband Rejections, IL = Insertion Loss
NG = Not given, Varac = Varactors, LC = Liquid Crystal, VO_2 = Vanadium Oxide, * = 3 dB FBW, $^{\&}$ = 10 dB FBW, $^{\#}$ = 15 dB FBW, $^+$ = 20 dB FBW

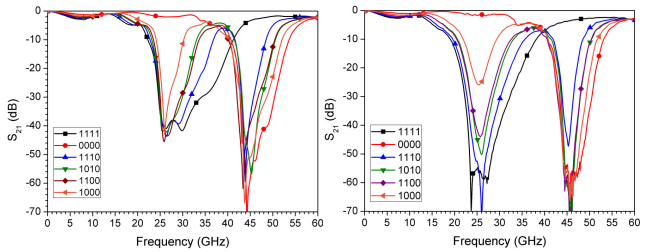

FIGURE 14. (a) Simulated and (b) measured insertion loss curves showing the bandwidth tuning capability of the proposed circuit with different switched states.

confirm that different switching patterns present different reactive loading profiles to the microstrip line resulting in different EBG characteristics in each unique switching state, as shown in Fig. 14(b). With these switching states, the proposed structure exhibits dual-band operation with tunable bandgap characteristics. For example, the fractional bandwidth for first stopband or band-1 can be tuned from 0 to 66.78% over a frequency range of 25.6 to 28.6 GHz with selectable bandstop rejection levels in a range of 1.8 dB to 55 dB with these six unique states. Similarly, bandwidth for band-2 can be tuned from 0 to 26.65% over a frequency range of 45.2 to 46.9 GHz with these switching states. The maximum insertion loss of 6.59 dB is observed between the stopbands at 39 GHz for '..1110..' state. A summary of bandgaps resulting from these switching states is presented in Table 3.

A comparison of the proposed filter structure with several reported reconfigurable bandstop filters is presented in Table 4. It can be seen that the proposed structure has many advantages as far as reconfigurable features such as stopband switching, dual-band operation with tunable stop bandwidths and resonant frequencies are concerned. In addition to these multiple adaptive features, the circuit also offers excellent rejection in the stopband, i.e., up to 55 dB, which is at least 20 dB deeper than other reported circuit topologies [3], [6], [9], [10], [12]–[15], [35], [39], [40]. Moreover, the proposed structure offers wider tuning ranges in resonant frequency and stop bandwidth for both bands, as compared to [9], [12], [13], [15], [35]. These features make the proposed structure a better choice for the reconfigurable filter design.

V. CONCLUSION

In this paper, a systematic design of a reconfigurable filter is presented that exhibits stopband switching, dual-band operation and tunable characteristics using a single reactive loading element in its unit cell. In the proposed unit cell, two spiral inductors have been introduced with a relatively smaller patch in the conventional shorted patch structures to achieve miniaturization in the MMIC environment. The

proposed mechanism offers a 28.3% wider stopband with a 62.6% compact size when compared to conventional shorted patch structures. A detailed account of the parasitic effects of active devices on the structure performance is presented with a comparison to ideal switching conditions. Simultaneously switching all the diodes in ON or OFF states results in band switching characteristics. The measured 10 dB stop bandwidth in the ON state is 66.8% at 28.6 GHz and in the OFF state is 26.6% at 46.9 GHz. Both have 55 dB rejections. The passband insertion loss is 1.8 dB and 3.1 dB at the two bandgap center frequencies. By individually controlling the switching state of each unit cell, dual stopband operation along with simultaneous tuning of bandgap characteristics can be achieved. The first and second stopband can be tuned from 0 to 66.8% and 0 to 26.6% bandwidths over frequency ranges of 25.6−28.6 GHz and 45.2−46.9 GHz, respectively. These features make the proposed reconfigurable EBG circuit a suitable candidate for different 5G and cognitive radio applications.

ACKNOWLEDGMENT

The authors would like to thank Dr. Evgeny Kuxa, Melissa Gorman, Gerry McCulloch, and Steve Hwang for measurements. They also thank WIN Semiconductor Corporation, Taiwan, for providing access to their PIH1-10 process.

REFERENCES

[1] J. Zhang, S. Zhang, Z. Ying, A. S. Morris, and G. F. Pedersen, "Radiation-pattern reconfigurable phased array with p-i-n diodes controlled for 5G mobile terminals," *IEEE Trans. Microw. Theory Techn.*, vol. 68, no. 3, pp. 1103–1117, Mar. 2020.

[2] S. N. Ali, P. Agarwal, L. Renaud, R. Molavi, S. Mirabbasi, P. P. Pande, and D. Heo, "A 40% PAE frequency-reconfigurable CMOS power amplifier with tunable gate-drain neutralization for 28-GHz 5G radios," *IEEE Trans. Microw. Theory Techn.*, vol. 66, no. 5, pp. 2231–2245, May 2018.

[3] E. A. Casu, A. A. Müller, M. Fernández-Bolaños, A. Fumarola, A. Krammer, A. Schüler, and A. M. Ionescu, "Vanadium oxide band-stop tunable filter for Ka frequency bands based on a novel reconfigurable spiral shape defected ground plane CPW," *IEEE Access*, vol. 6, pp. 12206–12212, 2018.

[4] G. Srivastava, A. Mohan, and A. Chakrabarty, "Compact reconfigurable UWB slot antenna for cognitive radio applications," *IEEE Antennas Wireless Propag. Lett.*, vol. 16, pp. 1139–1142, 2016.

[5] A. Alex-Amor, A. Palomares-Caballero, A. Palomares, A. Tamayo-Domínguez, J. M. Fernández-González, and P. Padilla, "Generalized director approach for liquid-crystal-based reconfigurable RF devices," *IEEE Microw. Wireless Compon. Lett.*, vol. 29, no. 10, pp. 634–637, Oct. 2019.

[6] C.-H. Ko, A. Tran, and G. M. Rebeiz, "Tunable 500–1200-MHz dual-band and wide bandwidth notch filters using RF transformers," *IEEE Trans. Microw. Theory Techn.*, vol. 63, no. 6, pp. 1854–1862, Jun. 2015.

[7] V. Lee, S. Lee, S. A. Sis, and A. Mortazawi, "Intrinsically switchable frequency reconfigurable barium strontium titanate resonators and filters," *IEEE Trans. Microw. Theory Techn.*, vol. 65, no. 9, pp. 3221–3229, Sep. 2017.

[8] L. M. Cano, A. L. Borja, V. E. Boria, and A. Belenguer, "Highly versatile coplanar waveguide line with electronically reconfigurable bandwidth and propagation characteristics," *IEEE Trans. Microw. Theory Techn.*, vol. 65, no. 1, pp. 128–135, Jan. 2017.

[9] T. Yang and G. M. Rebeiz, "Bandpass-to-bandstop reconfigurable tunable filters with frequency and bandwidth controls," *IEEE Trans. Microw. Theory Techn.*, vol. 65, no. 7, pp. 2288–2297, Jul. 2017.

[10] Z.-H. Chen, S.-X. Zhang, and Q.-X. Chu, "Dual-band bandstop filter with tunable lower stopband based on double-layer structure," *Microw. Opt. Technol. Lett.*, vol. 58, no. 9, pp. 2273–2276, 2016.

[11] Q. Li, X. Chen, P.-L. Chi, and T. Yang, "Tunable bandstop filter using distributed coupling microstrip resonators with capacitive terminal," *IEEE Microw. Wireless Compon. Lett.*, vol. 30, no. 1, pp. 35–38, Jan. 2020.

[12] S.-W. Jeong and J. Lee, "Frequency- and bandwidth-tunable bandstop filter containing variable coupling between transmission line and resonator," *IEEE Trans. Microw. Theory Techn.*, vol. 66, no. 2, pp. 943–953, Feb. 2018.

[13] W. Xu, Y. Zhang, Y. Peng, J. Wang, L. Mu, B. Yu, and H. Zhang, "Tunable bandstop HMSIW filter with flexible center frequency and bandwidth using liquid crystal," *IEEE Access*, vol. 7, pp. 161308–161317, 2019.

[14] Z.-H. Chen, S.-X. Zhang, and Q.-X. Chu, "Dual-band reconfigurable bandstop filter with independently controlled stopbands and constant absolute bandwidths," in *IEEE MTT-S Int. Microw. Symp. Dig.*, Jun. 2017, pp. 926–928.

[15] N. Kumar and Y. K. Singh, "RF-MEMS-based bandpass-to-bandstop switchable single- and dual-band filters with variable FBW and reconfigurable selectivity," *IEEE Trans. Microw. Theory Techn.*, vol. 65, no. 10, pp. 3824–3837, Oct. 2017.

[16] S. Y. Huang and Y. H. Lee, "Tapered dual-plane compact electromagnetic bandgap microstrip filter structures," *IEEE Trans. Microw. Theory Techn.*, vol. 53, no. 9, pp. 2656–2664, Sep. 2005.

[17] L. Yang, M. Fan, F. Chen, J. She, and Z. Feng, "A novel compact electromagnetic-bandgap (EBG) structure and its applications for microwave circuits," *IEEE Trans. Microw. Theory Techn.*, vol. 53, no. 1, pp. 183–190, Jan. 2005.

[18] A. M. E. Safwat, F. Podevin, P. Ferrari, and A. Vilcot, "Tunable bandstop defected ground structure resonator using reconfigurable dumbbell-shaped coplanar waveguide," *IEEE Trans. Microw. Theory Techn.*, vol. 54, no. 9, pp. 3559–3564, Sep. 2006.

[19] S. M. Moghadasi, A. R. Attari, and M. M. Mirsalehi, "Compact and wide-band 1-D mushroom-like EBG filters," *Prog. Electromagn. Res.*, vol. 83, pp. 323–333, 2008.

[20] I. Shahid, D. Thalakotuna, and M. Heimlich, "A bi-patch loaded microstrip line based 1-D periodic structure with enhanced stop bandwidth and band switching characteristics," *J. Electromagn. Waves Appl.*, vol. 33, no. 10, pp. 1329–1342, Jul. 2019.

[21] D. N. P. Thalakotuna, K. P. Esselle, L. Matekovits, M. Heimlich, and S. G. Hay, "Changing the electromagnetic bandgap and stopbands in a multistate periodic circuit," *Microw. Opt. Technol. Lett.*, vol. 55, no. 8, pp. 1871–1874, Aug. 2013.

[22] I. Shahid, D. Thalakotuna, D. K. Karmokar, and M. Heimlich, "Reactively loaded microstrip line based 1-D periodic structure with all-pass, low pass and stopband filter characteristics," in *Proc. 4th Austral. Microw. Symp. (AMS)*, Feb. 2020, pp. 1–2.

[23] L. Matekovits, M. Heimlich, and K. P. Esselle, "Tunable periodic microstrip structure on GaAs wafer," *Prog. Electromagn. Res.*, vol. 97, pp. 1–10, 2009.

[24] M. A. M. Hassan and A. A. Kishk, "Bandwidth study of the stacked mushroom EBG unit cells," *IEEE Trans. Antennas Propag.*, vol. 65, no. 8, pp. 4357–4362, Aug. 2017.

[25] A. B. Yakovlev, M. G. Silveirinha, O. Luukkonen, C. R. Simovski, I. S. Nefedov, and S. A. Tretyakov, "Characterization of surface-wave and leaky-wave propagation on wire-medium slabs and mushroom structures based on local and nonlocal homogenization models," *IEEE Trans. Microw. Theory Techn.*, vol. 57, no. 11, pp. 2700–2714, Nov. 2009.

[26] I. Shahid, D. N. Thalakotuna, D. K. Karmokar, and M. Heimlich, "Asymmetric transversal patch loaded microstrip line based 1-D periodic structure with flexible selection of stopband resonance," *AEU, Int. J. Electron. Commun.*, vol. 114, Feb. 2020, Art. no. 153010.

[27] D. M. Pozar, *Microwave Engineering*. Hoboken, NJ, USA: Wiley, 2009.

[28] E. B. Rosa, *The Self and Mutual Inductances of Linear Conductors*. Washington, DC, USA: U.S. Department of Commerce and Labor, 1908.

[29] Y. Lu, L. Shen, J. Wang, and Y. Shen, "The design of miniaturized broadband power divider utilizing GaAs-based IPD process and equivalent circuit model," *J. Semicond.*, vol. 38, no. 8, Aug. 2017, Art. no. 085004.

[30] G. Wei and Y. Zhiping, "Parameter extraction for 2-π equivalent circuit model of RF CMOS spiral inductors," *Chin. J. Semicond.*, vol. 27, no. 4, pp. 1–7, 2006.

[31] D. K. Karmokar, K. P. Esselle, and S. G. Hay, "Fixed-frequency beam steering of microstrip leaky-wave antennas using binary switches," *IEEE Trans. Antennas Propag.*, vol. 64, no. 6, pp. 2146–2154, Jun. 2016.

[32] Q. Zhang, X.-L. Tang, S. Hu, and Y. Chen, "A reconfigurable Goubau-line-based leaky wave antenna," in *Proc. 2nd URSI Atlantic Radio Sci. Meeting (AT-RASC)*, May 2018, pp. 1–3.

[33] I. Shahid, D. N. Thalakotuna, D. K. Karmokar, and M. Heimlich, "Band-stop filter synthesis scheme for reactively loaded microstrip line based 1-D periodic structures," *IEEE Access*, vol. 8, pp. 155492–155505, 2020.
[34] K. Song, W. Chen, S. R. Patience, Y. Chen, A. M. Iman, and Y. Fan, "Compact wide-frequency tunable filter with switchable bandpass and bandstop frequency response," *IEEE Access*, vol. 7, pp. 47503–47508, 2019.
[35] L. Kurra, M. P. Abegaonkar, A. Basu, and S. K. Koul, "Bandwidth reconfigurable bandstop filter using planar EBG structure," in *IEEE MTT-S Int. Microw. Symp. Dig.*, Dec. 2013, pp. 1–3.
[36] N. Zhang, Z. Deng, and F. Sen, "CPW tunable band-stop filter using hybrid resonator and employing RF MEMS capacitors," *IEEE Trans. Electron Devices*, vol. 60, no. 8, pp. 2648–2655, Aug. 2013.
[37] Z. Ge, L. Chen, L. Yang, R. Gómez-Garcia, and X. Zhu, "On-chip millimeter-wave integrated absorptive bandstop filter in (Bi)-CMOS technology," *IEEE Electron Device Lett.*, vol. 42, no. 1, pp. 114–117, Jan. 2021.
[38] V. N. R. Vanukuru and V. K. Velidi, "Compact millimeter-wave CMOS wideband three-transmission-zeros bandstop filter using a single coupled-line unit," *IEEE Trans. Circuits Syst. II, Exp. Briefs*, vol. 64, no. 9, pp. 1022–1026, Sep. 2017.
[39] V. N. R. Vanukuru and V. K. Velidi, "Millimeter-wave CMOS 30/80 GHz sharp-rejection dual-band bandstop filters using TFMS open-stepped-Impedance resonators," *IEEE Trans. Circuits Syst. II, Exp. Briefs*, vol. 68, no. 1, pp. 201–205, Jan. 2021.
[40] S.-C. Hsieh, C.-H. Chen, C.-C. Lin, and C.-C. Chang, "Design of millimeter-wave reconfigurable bandstop filter using CMOS-MEMS technology," in *Proc. 41st IEEE Eur. Microw. Conf.*, Oct. 2011, pp. 1095–1098.
[41] T. LaRocca, S.-W. Tam, D. Huang, Q. Gu, E. Socher, W. Hant, and F. Chang, "Millimeter-wave CMOS digital controlled artificial dielectric differential mode transmission lines for reconfigurable ICs," in *IEEE MTT-S Int. Microw. Symp. Dig.*, Jun. 2008, pp. 181–184.
[42] T. LaRocca, J. Liu, F. Wang, D. Murphy, and F. Chang, "CMOS digital controlled oscillator with embedded DiCAD resonator for 58–64 GHz linear frequency tuning and low phase noise," in *IEEE MTT-S Int. Microw. Symp. Dig.*, Jun. 2009, pp. 685–688.

IRFAN SHAHID (Member, IEEE) received the B.E. degree in avionics engineering from the National University of Sciences and Technology (NUST), Pakistan, in 2005, and the M.S. degree in computer science and technology from the University of Electronic Science and Technology of China (UESTC), Chengdu, China, in 2013. He is currently pursuing the Ph.D. degree with the Faculty of Science and Engineering, Macquarie University, Australia. His current research interests include EBG structures, reconfigurable circuits, impedance transformers, and circuits for microwave applications.

DUSHMANTHA N. THALAKOTUNA (Senior Member, IEEE) received the B.Sc. degree in electronics and telecommunication from the University of Moratuwa, Sri Lanka, in 2008, and the Ph.D. degree in electronic engineering from Macquarie University, Australia, in 2012. He has worked as a Radio Frequency Engineer and a Systems Engineer in both commercial and defence sector for over seven years. He is currently a Lecturer with the School of Electrical and Data Engineering, University of Technology Sydney, Australia. His current research interests include MMICs, Satcom antennas, base station antennas, reconfigurable microwave and millimeter wave circuits, and periodic structures.

DEBABRATA K. KARMOKAR (Senior Member, IEEE) received the B.Sc. degree in electrical and electronic engineering (EEE) from Khulna University of Engineering & Technology (KUET), Khulna, Bangladesh, and the Ph.D. degree in electronic engineering from Macquarie University, Sydney, NSW, Australia.

In 2007, he joined KUET as a Lecturer, where he was promoted to an Assistant Professor and also served as an Assistant Director for the Students' Welfare of the university. From 2012 to 2015, he was a Casual Academic, a Research Assistant, and the Secretary of the IEEE Student Branch at Macquarie University. From 2016 to 2019, he was a Postdoctoral Research Associate with the Global Big Data Technologies Centre (GBDTC), University of Technology Sydney (UTS), Australia. From 2019 to 2020, he was a Lecturer with the School of Engineering, Macquarie University. In 2020, he joined the University of South Australia (UniSA), SA, Australia, as a Lecturer, where he is currently the Program Director of UniSA STEM.

Dr. Karmokar is serving as the Counselor for the IEEE UniSA Student Branch. He was a recipient of several scholarships and research grants. In addition, he has received a number of awards, including the Young Scientist Award from the Venus International Foundation, in 2018, and the URSI Young Scientist Award, in 2019. He is serving as a reviewer for several journals of IEEE, IET, Wiley, MDPI, Hindawi, Taylor & Francis, Springer, and Elsevier, and an Associate Editor for IEEE Access.

SIMON J. MAHON received the B.Sc., B.E. (Hons.), and Ph.D. degrees from The University of Sydney, in 1985, 1987, and 1993, respectively.

From 1993 to 2017, he has designed, and led design teams, creating scores of successful III-V products for various applications. In 2018, he was appointed as an Industry Professor with Macquarie University. He has over 75 refereed publications, including a book chapter, five patents, and many journal and conference proceedings.

MICHAEL HEIMLICH (Senior Member, IEEE) received the B.S. *(magna cum laude)*, M.E., and Ph.D. degrees from the Rensselaer Polytechnic Institute, Troy, NY, USA. He joined Macquarie University, Sydney, in 2009, after 25 years in industry, where he is currently a Professor with the School of Engineering. His current research interests include mm-wave reconfigurable electronics and formal methods in RF/microwave design.